Original Article

Diamond-based neutron scatter camera

Ahmed Alghamdi [a, b], Eric Lukosi [b, *]

[a] Nuclear Science Research Institute, King Abdulaziz City for Science and Technology, Riyadh, Saudi Arabia
[b] Department of Nuclear Engineering, University of Tennessee, Knoxville, TN, 37922, USA

A R T I C L E   I N F O

A B S T R A C T

In this study, a diamond-based neutron scatter camera (DNSC) was developed for neutron spectroscopy in high flux environments. The DNSC was evaluated experimentally and through simulations. It was simulated using several Monte Carlo codes in a two-array layout. The two-array model included two diamond detectors. The simulation reconstructed the spectra of ^{252}Cf and ^{239}Pu—Be neutron sources with high accuracy (~93%). The two-diamond array system was experimentally evaluated, demonstrating the neutron spectroscopy capabilities of the DNSC. The reconstructed spectrum of the ^{239}Pu—Be source manifested the characteristic peaks of the source. The advantage of a DNSC over a NSC is its ability to define any neutron double-scattering events without the need to absorb incident neutrons in the second detector, and atomic recoil energy information is not needed to determine the incident neutron energy.

1. Introduction

The diamond-based neutron scatter camera (DNSC) proposed in this study leverages the advantageous characteristics of diamond detectors, such as compact size, extremely fast-rise signals, and radiation hardness [1–4]. In addition, diamond detectors are capable of providing fast neutron measurements [5,6]. The DNSC system is intended to operate in harsh neutron radiation environments such as fission and fusion reactors, with high reliability. Furthermore, the compact DNSC system can be utilized in neutron spectroscopy for space missions. The proposed DNSC system was designed for spectral analysis based on a large set of Monte Carlo simulations. Additionally, it was investigated experimentally to prove the diamond NSC concept and validate the simulation results.

The NSC was first proposed by Mascarenhas et al. for locating special nuclear materials (SNM) sources for homeland security purposes [7]. The SNM source spectrum was identified based on reconstructed fast fission neutrons and plotted using the time-of-flight (ToF) of neutron double-scattering events. The NSC comprises two parallel panels, each with four liquid scintillators. The pulse shape discrimination processing method was utilized for (n-γ) discrimination because the SNM sources emitted photons in

addition to neutron particles [8]. The neutron source origin was located by developing the probability cones of the scattered neutrons, as shown in Fig. 1.

For spectral analysis, the incident neutron energy (E_n, MeV) can be calculated based on the energy deposited by the recoil proton (E_p, MeV) and the ToF of the scattered neutron (E'_n, MeV) that traveled between two of the scintillation detectors. The scattered neutron energy can be calculated using Equation (1), wherein m_n is the rest mass of the neutron (939.565 MeV) and d is the known separation distance [9]:

$$E'_n = \frac{m_n}{2}\left(\frac{d}{ToF}\right)^2 \tag{1}$$

Next, the recoil proton energy can be determined using Equation (2) as follows:

$$E_p = E'_n \tan(\theta)^2 \tag{2}$$

where θ is the scattering angle of the deflected neutron relative to the incident neutron direction in the lab frame. Then, the incident neutron energy is obtained based on the law of the conservation of
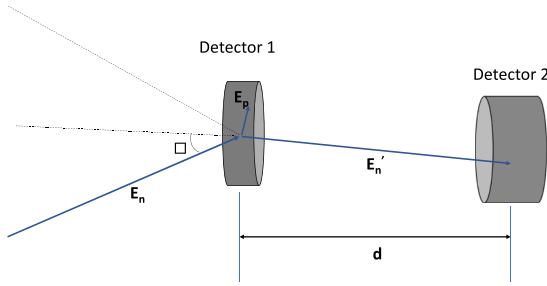

Fig. 1. Back-projection scheme for a double neutron scattering event.

energy:

$$E_n = E_p + E'_n. \tag{3}$$

Krenz et al. successfully pinpointed a ^{252}Cf source that was 30 m away from a more advanced NSC [10]. The detection threshold was set as 70 keVee to prevent noise, and a 120° angle of view was recorded for their NSC. The system demonstrated an angular resolution (1σ) of 12° and the capability to reconstruct neutron energy in the range of 0.5–10 MeV.

The NSC detection efficiency was improved by increasing the number of liquid scintillator detectors (EJ-309) per panel from 9 to 16. In this improved system, the separation distance between the two panels was adjustable (13–127 cm), and the shortest distance (13 cm) achieved the highest detection efficiency. By contrast, a separation distance of 127 cm provided the best angular resolution. The energy resolution of a reconstructed mono-energetic neutron (2.5 MeV) was recorded as 10–15% (non-Gaussian peak shape) when the spacing between the two panels was 40 cm. The substantial detector thicknesses of 5 cm and 13 cm for the front and back panels, respectively, reduced the energy resolution of the system. By contrast, the increased number of NSC elements increased the angular resolution (~10°) compared with that in the previous NSC design [11,12]. However, the large size and poor energy resolution of organic liquid scintillators have remained unresolved drawbacks of NSC systems.

In this paper, Section 2 provides the details of the DNSC theory and simulation developed in this study and the factors used to define the optimum designs of the DNSC; information regarding the experimental setup is also provided. Section 3 presents the analysis of the DNSC simulation spectroscopic results as well as the experimental results. Section 4 provides the conclusions and suggestions for future work.

2. Materials and methods

2.1. Two-diamond array

The law of conservation of energy was applied to the energy of the elastic neutron scattering to determine the energy of the scattered neutron. The energy of the incident neutrons was determined using the known separation distance, d, and the ToF based on the travel time between the two detectors.

$$\gamma^2 = \frac{1}{(1-\beta^2)} = \frac{1}{\left(1 - \left[\frac{\left(\frac{d}{ToF}\right)}{c}\right]^2\right)} \tag{4}$$

From the calculation of the Lorentz factors, the energy of the

scattered neutron traveling between the first and second detectors was obtained as

$$E'_n = (\gamma - 1)*m_n, \tag{5}$$

where E'_n is the scattered neutron energy, and m_n is the mass of the neutron. The incident neutron energy (E_n) was then determined using relativistic kinematics, as shown in Equation (6), where ϑ is the scattering angle of the neutron [13].

$$E_n = \frac{E'_n*(A+1)^2}{\left[\cos\vartheta - \sqrt{A^2 + \sin\vartheta^2}\right]^2} \tag{6}$$

One advantage of a two-diamond array over the current NSC is the lack of the need to absorb the incident neutrons in the second layers of the diamond because the angle between the diamond detectors is small and known. However, the neutron source is assumed to be a monodirectional source, and the energy deposition must be greater than the threshold (10 keV). In addition, in contrast to the NSC, the DNSC utilized relativistic kinematics because it exhibited a slightly better reconstructed neutron energy than with non-relativistic calculations, particularly in the fast neutron range.

Once the neutron energy spectrum was constructed in the DNSC system, it required the correction of the changes in the scattering cross-section of the carbon atom. The neutron scattering cross-section and angular distribution vary as a function of energy. Fig. 2 shows the relationship among the angular distribution, neutron recoil angle, and neutron energy using the CENDL-3.1 ENDF neutron library [14]. The neutron spectrum could then be corrected based on the obtained neutron energy spectrum and detector efficiency.

2.2. Monte Carlo simulation

The DNSC design simulations were performed using the Monte Carlo N-Particle (MCNP6.1) simulation software with the ENDF/B-VII.1 library [15]. The MCNP simulation generates an output file called PTRAC that provides the history of the interaction of the neutrons, including the secondary particles, with the diamond sensors. However, only elastic neutron scattering interactions were
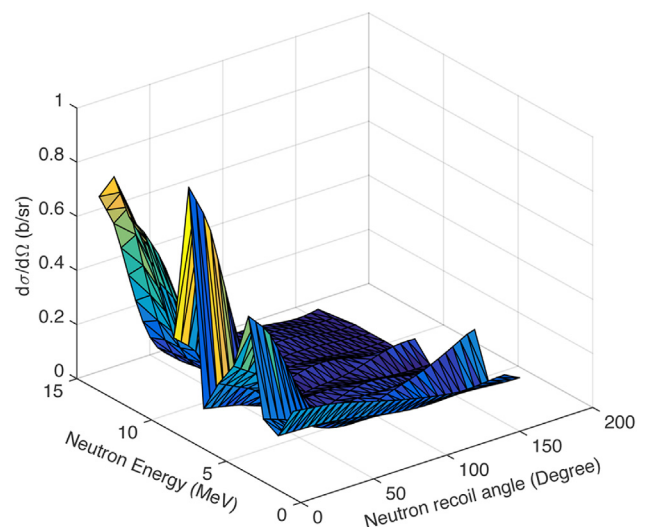

Fig. 2. Relationship among the angular distribution, neutron recoil angle, and neutron energy in the interaction with a carbon atom. The plot was generated from the CENDL-3.1 ENDF neutron library [14].
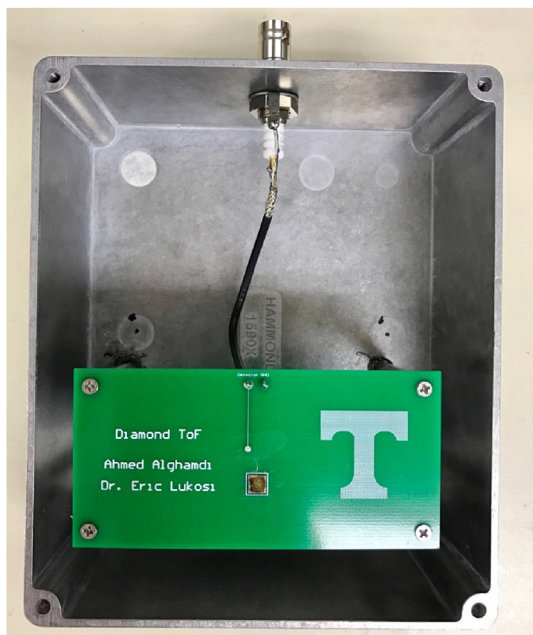
Fig. 3. Aluminum enclosure.

addressed by the DNSC because it is based solely upon energy conservation. Post-processing codes were developed to extract the details of any successful double elastic scattering.

The geometry of the diamond detectors was modeled based on the typical size of commercial electronic-grade diamond sensors (0.5 cm × 0.5 cm × 0.05 cm). All the simulated diamonds were surrounded by air to mimic the experimental environment. Various mono-energetic point sources (0.25–14 MeV) represented the neutron sources. The angles between the diamond detectors were determined for multiple DNSC orientations, based on factors including detection efficiency, energy, and angular resolution. Once the angles between the diamonds were defined, the optimum separation distance was selected based on the best energy resolution that could be obtained while maintaining acceptable detection

efficiency.

After defining the optimum DNSC orientations based on the energy resolution and timing uncertainty, two neutron sources (^{252}Cf and ^{239}Pu−Be) were modeled as the point sources to demonstrate the capability of the DNSC. A bare ^{252}Cf fission neutron source was generated through the source card option in the MCNP6 software [15], and the ^{239}Pu−Be neutron source was developed based on the data in Ref. [16].

A two-diamond array system configuration was implemented in a series of MCNP simulations. The system was constructed to evaluate the capability of the DNSC to provide neutron spectroscopy measurements.

2.3. Experimental setup

A two-diamond array was fabricated to verify its neutron spectroscopy capabilities experimentally. Two electronic-grade diamond detectors (0.45 cm × 0.45 cm × 0.05 cm) were cleaned and metalized with conductive layers to achieve ohmic resistive contact. Furthermore, 50/100 nm Cr/Au metallization contacts were deposited on both surfaces of the diamond detectors using DC and RF sputtering, respectively. Then, the diamond detectors were thermally annealed for 20 min in argon gas, heated to 600 °C, to acquire better ohmic contact properties [17]. The ohmic contact exhibits a linear current-voltage (I−V) curve to maintain a low resistance in order to allow charge to flow easily in both directions between the Cr/Au conductive layer and the diamond [18]. After metallization, each diamond was mounted on a read-out printed circuit board. As shown in Fig. 3, each diamond detector was contained within an electrical housing and mounted onto an extruded aluminum frame. The frame allowed the relative orientation between the two diamond detectors to be controlled. Because the enclosures were thick enough to increase the number of scattered neutrons, both the front and rear sides of the boxes were cut away, and the cut areas were covered with aluminum foil.

In addition to the diamond sensors, two CIVIDEC C6 fast amplifiers and a CAEN digitizer V5730 captured the ToF of the double-scattering events, as shown in Fig. 4. The fast pulse-shaping amplifier produced a fast signal with a Gaussian shape (full width at half maximum (FWHM) = 10 ns). The digitizer had a fast sampling rate of 500 MHz and a useful GUI interface. It was operated in
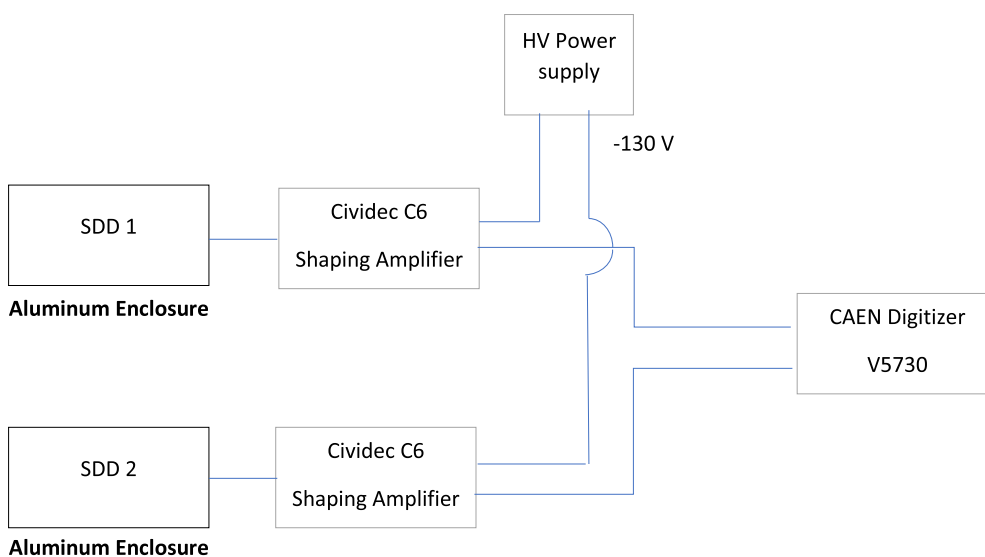

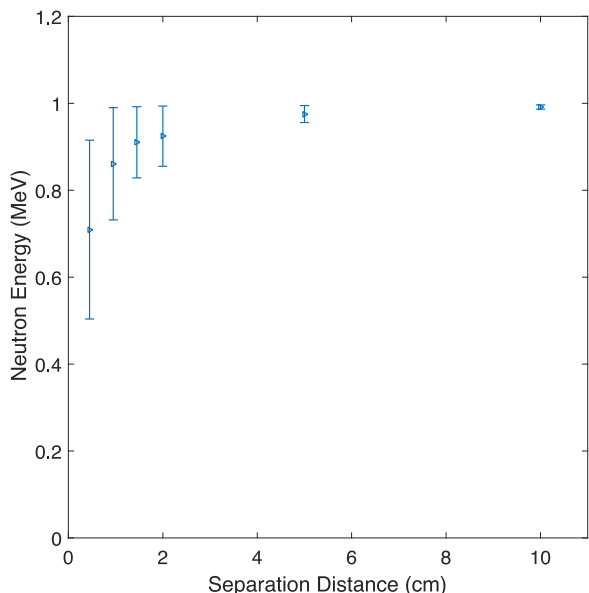**Fig. 4.** Electronic block diagram of the two-diamond NSC system.

Fig. 5. 1 MeV neutron energy reconstructed by the two-diamond system for different separation distances.

Fig. 7. Detection efficiency and energy resolution of the two-diamond array system.

the coincidence mode and recorded all events within a timing window of 20 ns using CAEN Compass software. The generated files included the time stamp in picoseconds, and other signal information were processed offline.

3. Results and discussion

3.1. MCNP results

Mapping the system sensitivity in the simulation space to fast mono-energetic neutrons indicated that the angle between the two diamond detectors strongly affected the energy sensitivity range of the two-array diamond NSC. The separation distance was evaluated based on the accuracy of the reconstructed energy of a 1 MeV mono-energetic neutron. Fig. 5 shows the uncertainties of the reconstructed incident neutron for a range of separation distances.
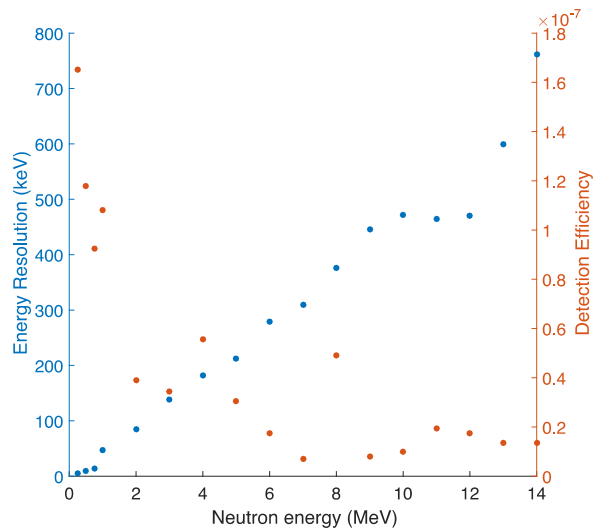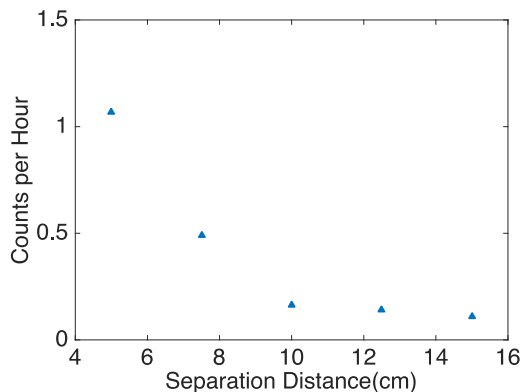

Fig. 8. Two-diamond NSC system double elastic scattering counts per hour for an isotropic 239Pu–Be source.

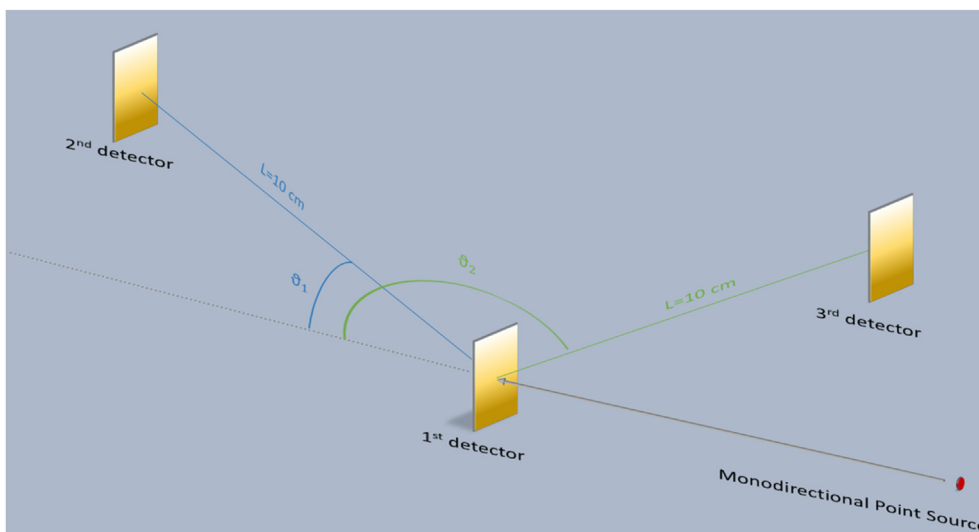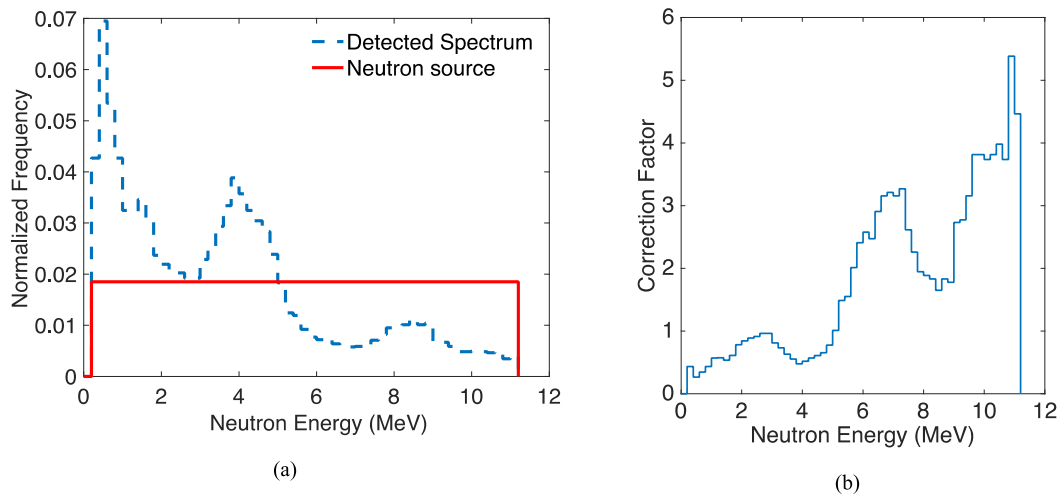**Fig. 6.** Two-diamond array NSC setup.

(a)

(b)

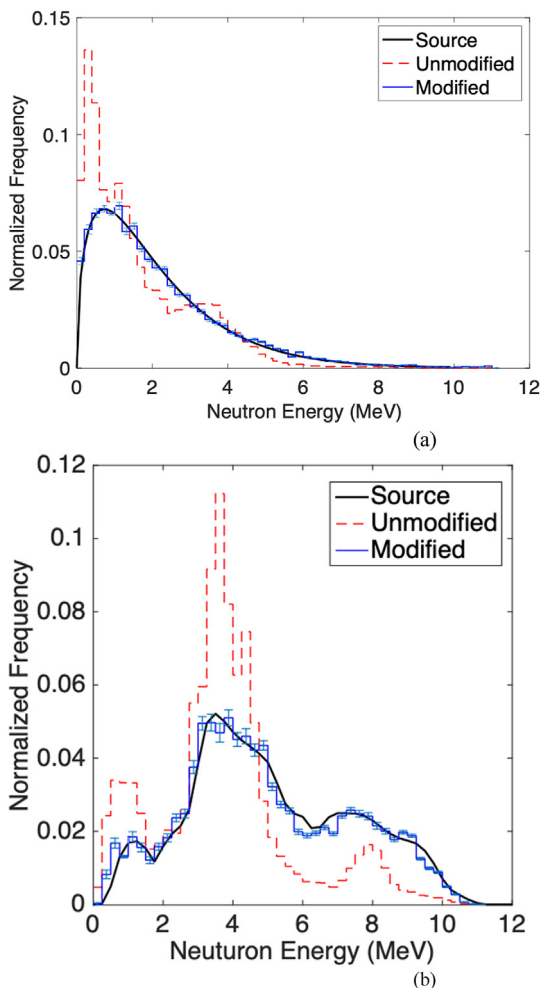**Fig. 9.** Neutron source: (a) Simulated and obtained spectra; (b) Correction factor.

(a)

(b)

Fig. 10. Spectra of the (a) ^{252}Cf and (b) ^{239}Pu−Be source reconstructed by the two-diamond NSC.

The first diamond detector was fixed, while the second diamond had two positioning options to provide higher detection efficiency. The two-diamond array NSC was simulated as three diamond detectors instead of separately determining each position of the

second diamond. A multitude of detection geometries was simulated, revealing that the most efficient detection and highest energy resolution were achieved using three 0.5 cm × 0.5 cm × 0.05 cm diamond detectors separated by 10 cm. For incident neutron energies below 1 MeV, the angle that maximized the detection threshold was 160°. For neutrons at or above 1 MeV, the best scattering angle was defined as 45° based on the simulation results (see Fig. 6).

As discussed in the previous section, both the energy resolution and detection efficiency of the system were defined through simulation, as shown in Fig. 7. The detection efficiency was significantly low owing to the small size of the diamond detectors and the need for double-scattering events and relatively large separation distances to achieve acceptable energy resolution. The proportional relationship between the energy resolution and detection efficiency is also shown in Fig. 7.

The MCNP code was utilized to obtain the counts per hour for an isotropic ^{239}Pu−Be source to define the detection efficiency of the two-diamond NSC for later experimental work. The source was located 50 cm from the detection system and modeled as an isotropic point source with a neutron emission rate of 2.4×10^6 neutrons per second, which is similar to the neutron emission rate of the Monsanto Research Corporation ^{239}Pu−Be source [19]. Fig. 8 displays the counts per hour for each separation distance.

The correction factor (CF) was essential for accurately reconstructing the neutron energy spectrum from the measured response, as previously described. The MCNP software was utilized to define the CF for any neutron source, where the CF represented the multiplication factor necessary to reconstruct the actual neutron source energy spectrum. The two-diamond array geometry was modeled with a neutron source that had a single-energy bin spectrum, i.e., the incident neutron was set as one histogram bin with a range of 0.2−11.6 MeV (see Fig. 9a). After the simulation was complete, the CF was determined for each histogram bin as the ratio between the reconstructed spectrum and the neutron source value, as shown in Fig. 9b.

For the two poly-energetic neutron sources used in this study, the two-diamond array NSC matched the incident neutron spectrum well. The results for the ^{252}Cf fission neutron source and ^{239}Pu−Be source are shown in Fig. 10 a and b, respectively. Both sources were shown before (unmodified) and after applying the CF (modified), respectively. After they were adjusted by applying the CF, the neutron spectra agreed with the neutron sources better than
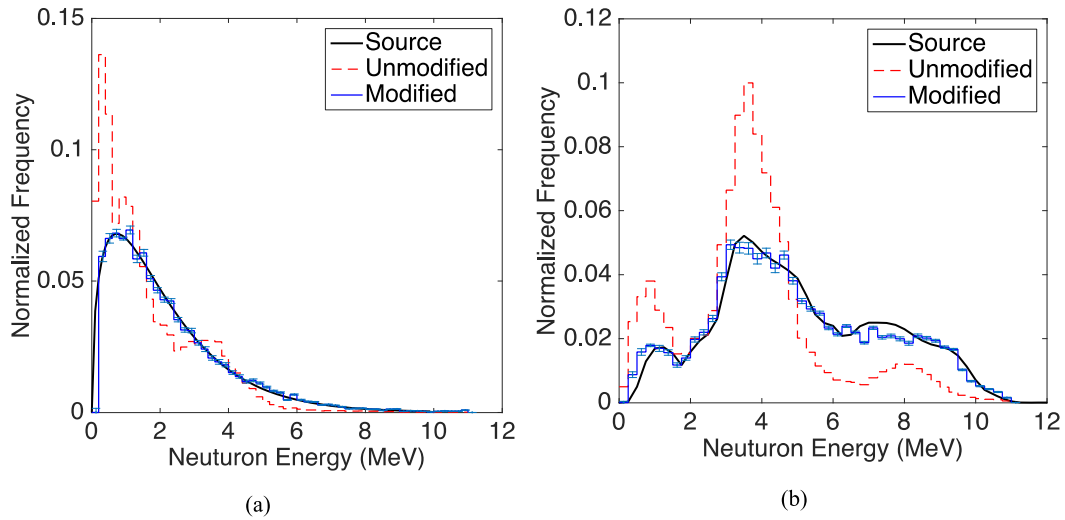
Fig. 11. Spectra of the (a) ^{252}Cf and (b) ^{239}Pu−Be source reconstructed by the 16-pixel two-diamond array.
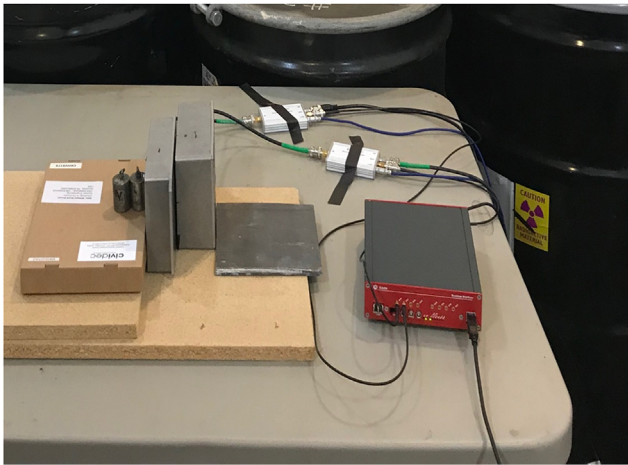

Fig. 12. Arrangement of the two-diamond array NSC experiment.

when unmodified. However, the higher energy range (5−7 MeV) of the modified spectrum for the ^{239}Pu−Be neutron source showed some variances due to low counts.

The simulated number of neutrons of ^{252}Cf (3×10^{11}) was equivalent to 6 h of neutron emission by a ^{252}Cf isotropic source with a neutron emission rate of 2.314×10^{10} n/s located 50 cm away from the detection system [20]. For the isotropic ^{239}Pu−Be source, the emission rate was defined as 2.4×10^{6} n/s, based on the expected neutron emission rate of the University of Tennessee ^{239}Pu−Be source, and the 10 cm distance between the source and the first diamond [19]. The expected measurement time would be extremely long—approximately 97 days—owing to the low detection efficiency of the system.

A 16-pixel two-diamond system was also simulated to increase detection efficiency and energy resolution. Each pixel was 1.25 mm $\times$ 1.25 mm. The separation distance between the diamond plates was reduced to 5 cm to achieve higher detection efficiency while maintaining acceptable energy resolution. Fig. 11 provides the reconstructed incident neutron spectrum for each neutron source, with and without the application of the CF. The 16-pixel two-diamond array also provided satisfactory agreement between
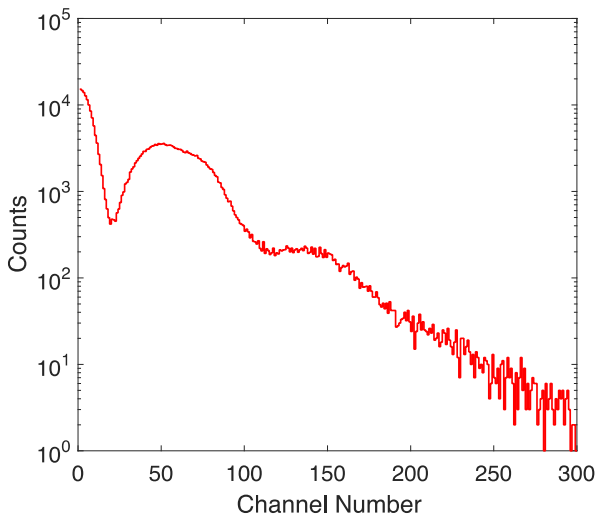

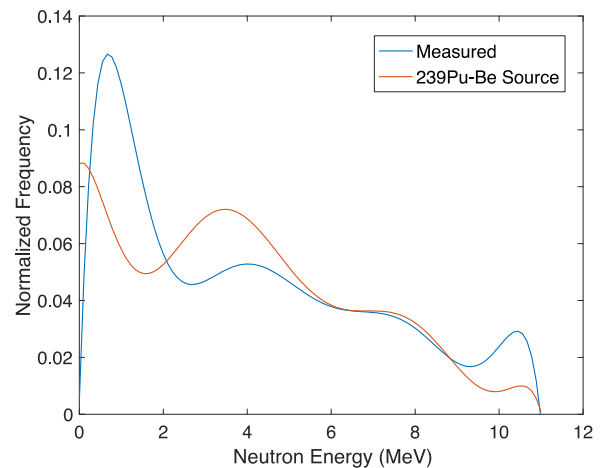**Fig. 13.** Pulse-height spectrum of a ^{239}Pu−Be source in the second diamond detector.

Fig. 14. Reconstructed neutron spectrum of the ^{239}Pu−Be source.

the spectra of the incident neutron sources.

3.2. Experimental results

Two bare ^{239}Pu−Be neutron sources were used in this study. Each source had a neutron emission rate of 2.4×10^6 neutrons per second. Because of the nature of isotropic sources and the proximity between the second diamond detector and the neutron sources, measurements were performed only for the 45° position. Additionally, the sources were aligned and placed 2 cm from the first diamond sensor. A greater separation distance would be required to obtain monodirectional neutrons, and, thus, better energy resolution. However, owing to time limitations, both sources were maintained in their positions to obtain more neutrons. For the same reason, the separation distance was reduced to from 10 cm to 5 cm. All the electronics were placed on a wooden panel to decrease vibration (see Fig. 12).

The constant fraction discriminator (CFD) mode was initially used for the measurements to obtain satisfactory timing resolution. However, after three days, the system had an insignificant number of counts, which were mostly saturation counts. Consequently, the leading-edge discriminator (LED) mode was selected with a 60 least significant bit threshold to avoid low noise signals. The pulse-height spectrum was measured for the second diamond, as shown in Fig. 13; because it was further from the sources, it had fewer gamma-ray interactions than that of the first detector.

The two-peak interaction of the inelastic scattering of ^{12}C(nα)^{9}Be and ^{12}C(n,n')3α was prominent in center channels 60 and 150, respectively. However, the first peak was wider owing to the elastic scattering of the wide neutron spectrum of the ^{239}Pu−Be source.

The experiment was performed for a total of 370 h. The output data were processed offline using the MATLAB code developed to read both files and determine the ToF data for each interaction. Based on previous neutron ToF calculations for the ^{239}Pu−Be source, the MATLAB code accepted only events with a ToF in the range of 1−7.2 ns. The ToF range was calculated for the upper and lower neutron energies of the ^{239}Pu−Be source based on the 5 cm separation distance. Additionally, the code extracted only events that had a reasonable time-stamp flag. The final step was converting the measured ToF into an energy histogram and modifying it by applying the simulated CF. Fig. 14 provides a comparison of the modified and expected neutron source spectra [21].

The neutron spectrum of the ^{239}Pu−Be source primarily depended on the masses and weight fractions of the Pu isotopes within it, which were undefined. In addition, the ^{239}Pu−Be sources were manufactured in 1960; therefore, significant growth of daughter nuclei had occurred. The high decay constant of the daughter nuclide (^{241}Am) increased the (α,n) interaction rates and, consequently, the neutron yields of the sources [22]. Therefore, the current neutron spectra of the sources used in this study might have differed slightly from the expected spectra. However, the experimental results did match the peak neutron energy regions of the ^{239}Pu−Be neutron spectrum.

For low neutron energies (<2 MeV), the reconstructed spectra did not match well, due to the use of the 45° diamond for these low energies. In addition, high gamma-ray interaction could lead to false counts at low energies. However, the two-array system spectrum matched the peaks centered at 4, 8, and 10.5 MeV. Slight differences between the reconstructed and source spectra resulted from uncertainties in the reconstructed neutron energies for the low separation distance (5 cm), as indicated by the simulation results. In addition, false counting could be caused by gamma rays or by inelastic or absorption interactions of the neutrons with carbon atoms, beside the neutrons interacting with the surrounding surfaces of the experimental setup.

4. Conclusions

In this study, the capability of a two-diamond array NSC to reconstruct the spectra of incident neutron sources was demonstrated experimentally and through simulation. In contrast to all other NSCs, the two-diamond array requires a smaller diamond size to reconstruct the neutron energy without the need to absorb incident neutrons in the second detector. Additionally, the atomic recoil energy information is not needed to determine the incident neutron energy. The two-diamond array NSC provided a reconstructed spectrum superior to those in recent studies of a plastic scintillator NSC [13]. The simulated two-diamond array NSCs identified ^{252}Cf and ^{239}Pu−Be neutron sources with high accuracy (~93%). The 16-pixel, two-diamond array system provided good agreement with the incident neutron source spectra. Furthermore, the system demonstrated a detection efficiency that was an order of magnitude better than that of similar systems with non-pixelated diamond sensors. As expected, angular and depth uncertainties significantly affected the energy resolution.

During the experiment, the proposed two-diamond system demonstrated all the characteristic peaks of the ^{239}Pu−Be neutron source. Specifically, the measurements matched the 8 and 10.5 MeV source peaks. The two-diamond system DNSC is sufficient for neutron spectroscopy in harsh neutron environments, such as fusion reactors, which generate extremely intense neutron flux, or space missions, where small size and low weight are crucial.

Declaration of competing interest

The authors declare that they have no known competing financial interests or personal relationships that could have appeared to influence the work reported in this paper.

References

[1] R.S. Balmer, et al., Chemical vapour deposition synthetic diamond: materials, technology and applications, J. Phys. Condens. Matter 21 (36) (2009) 364221, https://doi.org/10.1088/0953-8984/21/36/364221.

[2] W. De Boer, et al., Radiation hardness of diamond and silicon sensors compared, Phys. Status Solidi A 204 (9) (2007) 3004−3010, https://doi.org/10.1002/pssa.200776327.

[3] J. Isberg, et al., High carrier mobility in single-crystal plasma-deposited diamond, Science 297 (5587) (2002) 1670−1672, https://doi.org/10.1126/science.1074374.

[4] G. Schmid, et al., A neutron sensor based on single crystal CVD diamond, Nucl. Instrum. Methods Phys. Res., Sect. A 527 (3) (2004) 554−561, https://doi.org/10.1016/j.nima.2004.03.199.

[5] M. Pillon, et al., Experimental response functions of a single-crystal diamond detector for 5−20.5 MeV neutrons, Nucl. Instrum. Methods Phys. Res., Sect. A 640 (1) (2011) 185−191, https://doi.org/10.1016/j.nima.2011.03.005.

[6] M. Rebai, et al., Pixelated single-crystal diamond detector for fast neutron measurements, J. Instrum. 10 (3) (2015) C03016, https://doi.org/10.1088/1748-0221/10/03/C03016.

[7] N. Mascarenhas, et al., Development of a neutron scatter camera for fission neutrons, in: IEEE Nucl. Sci. Symp. , San Diego, California, Oct. 29- Nov. 4, 2006, https://doi.org/10.1109/NSSMIC.2006.356135.

[8] M.L. Roush, M.A. Wilson, W.F. Hornyak, Pulse shape discrimination, Nucl.

Instrum. Methods 31 (1) (1964) 112−124, https://doi.org/10.1016/0029-554X(64)90333-7.

[9] G.F. Knoll, Radiation Detection and Measurement, forth ed., John Wiley & Sons, New York, 2010.

[10] K.D. Krenz, et al., Results with the Neutron Scatter Camera, Sandia National Lab ,(SNL-CA), Livermore, CA (United States), 2008. SAND−2008-6699C.

[11] E. Brubaker, et al., Measurement of the Fast Neutron Energy Spectrum of an 241Am-Be Source Using a Neutron Scatter Camera, Sandia National Lab ,(SNL-CA), Livermore, CA (United States), 2011, pp. SAND2011−2806J470536.

[12] N. Mascarenhas, et al., Results with the neutron scatter camera, IEEE Trans. Nucl. Sci. 56 (3) (2009) 1269−1273, https://doi.org/10.1109/TNS.2009.2016659.

[13] J.K. Shultis, R.E. Faw, Fundamentals of Nuclear Science and Engineering, third ed., CRC press, New York, 2016.

[14] Z.G. Ge, et al., The updated version of Chinese evaluated nuclear data library (CENDL-3.1), J. Kor. Phys. Soc. 59 (2) (2011) 1052−1056, https://doi.org/10.3938/jkps.59.1052.

[15] T. Goorley, et al., Initial MCNP6 release overview, Nucl. Technol. 180 (3) (2012) 298−315, https://doi.org/10.13182/NT11-135.

[16] Z.R. Harvey, Neutron Flux and Energy Characterization of a Plutonium-Beryllium Isotopic Neutron Source by Monte Carlo Simulation with Verification by Neutron Activation Analysis, Master Diss, University of Nevada, Las Vegas, 2010.

[17] T.G. Wulz, Advanced Radiation Detection Devices: 3D Diamond Detectors and KSr2I5: Eu Scintillating Crystals, PhD Diss, University of Tennessee, Knoxville, 2017.

[18] D.A. Neamen, Semiconductor Physics and Devices, forth ed., McGraw-Hill, New York, 2012.

[19] M.E. Anderson, Neutron Energy Spectra of 239 PuBe, 238pu_F, and 238Pu180 (A,n) Sources. MLM-1422 vol. 34, Mound Laboratory, Monsanto Research Corporation, October 31, 1967, p. 38.

[20] F.T. Corporation, Cf-252 neutron source, Available from: https://www.frontier-cf252.com/neutron-sources/, 2015.

[21] M.E. Anderson, R.A. Neff, Neutron energy spectra of different size 239Pu Be (α, n) sources, Nucl. Instrum. Methods 99 (2) (1972) 231−235, https://doi.org/10.1016/0029-554X(72)90781-1.

[22] G.M.X. Ghita, Comprehensive Modeling of Special Nuclear Materials Detectionusing Three-Dimensional Deterministic and Monte Carlo Methods, PhD diss, University of Florida, Gainesville, 2008.